Oral presentation | Higher order methods

Higher order methods-II

Tue. Jul 16, 2024 10:45 AM - 12:45 PM Room C

[4-C-02] High-order Compact Gas-kinetic Scheme on Structured and Unstructured Meshes for Compressible Flow Simulations

*Fengxiang ZHAO[1], Kun XU[1,2] (1. Department of Mathematics, The Hong Kong University of Science and Technology, 2. Department of Mechanical and Aerospace Engineering, The Hong Kong University of Science and Technology)

Keywords: high-order compact scheme, direct numerical modelling, gas-kinetic scheme

High-order Compact Gas-Kinetic Scheme on Structured and Unstructured Meshes for Compressible Flow Simulations

Fengxiang ZHAO* and Kun XU*,**
Corresponding author: makxu@ust.hk
* Department of Mathematics, Hong Kong University of Science and Technology (HKUST), Clear Water Bay, Kowloon, Hong Kong.
** Department of Mechanical and Aerospace Engineering, HKUST, Clear Water Bay, Kowloon, Hong Kong.

Abstract: Developing high-order numerical schemes for compressible flow simulations is challenging, particularly when it comes to resolving high-wavenumber waves and capturing strong shock waves simultaneously. Recently, a high-order compact gas-kinetic scheme (GKS) has been developed based on a time-accurate evolution model. This approach integrates both numerical accuracy and physical consistency through the direct modeling of gas evolution in a discretized space. The compact GKS has proven to be exceptionally robust and is capable of employing a large explicit time step, significantly larger than those used in many conventional compact methods. The construction of the compact GKS is characterized by several key components: 1. High-order compact spatial reconstruction with only adjacent cells. This involves updating cell-averaged flow variables and their gradients using high-order time-accurate gas evolution model. A nonlinear limiter is designed in the high-order time derivatives of the flux function. 2. Flow variable evolution. This accounts for possible discontinuities at the cell interface to update reliable cell-averaged gradients. These unique features underpin the robustness and accuracy of the compact GKS. In summary, the high-order compact GKS relies solely on the high-order evolution model, distinguishing it from compact schemes based on the first-order Riemann solver.

Keywords: High-Order Compact Scheme, Direct Numerical Modeling, Gas-Kinetic Scheme, Compressible Flow Simulations.

1 Introduction

The development of high-order compact schemes for compressible flow simulations has gained significant attention in recent decades, leading to a wide array of methods, including discontinuous Galerkin (DG) methods [1, 2, 3], correction procedure via reconstruction (CPR) method [4, 5], compact finite difference schemes [6] and compact finite volume schemes [7, 8]. However, a clear and unifying principle for constructing such schemes has not been defined. Existing high-order compact schemes often encounter difficulties and exhibit suboptimal performance, particularly in simulations involving shock waves. The design of intricate trouble cell detection algorithms and nonlinear limiters has become commonplace in the pursuit of robust high-order compact schemes.

Constructing high-order compact schemes has traditionally been challenged by the difficulty in defining physically consistent evolution equations for degrees of freedom within a cell, especially for discontinuous solutions like strong shock waves. This study introduces a novel framework for constructing compact schemes, emphasizing the use of time-accurate dynamic evolution models. Employing a time-dependent solver, such as the gas distribution function from the GKS used here, allows for capturing the time-dependent evolution within a time step from a piecewise polynomial initial condition. This approach naturally couples space and time, reflecting spatial inhomogeneity and unsteady dynamic effects in the evolution solution. Projecting this solution yields not only cell averages but also crucial higher-order spatial information, such as averages of derivatives, for constructing high-order compact schemes.

In the current framework for compact schemes, cell averages and their gradients of flow variables are updated using fluxes and flow variables obtained from the time-accurate evolution model at cell interfaces. Two key components are crucial for the accuracy and robustness of these updates. High-order time evolution model with the nonlinear limiter imposed on the high-order time derivatives of

the flux function. This approach mitigates oscillations caused by the high-order discretization in time, particularly in the presence of shock waves crossing cell interfaces within a time step. Independent evolution of flow variables on both sides of a cell interface: This component accounts for the potential presence and propagation of discontinuities within a cell during a time step. This ensures robustness and accuracy of updating cell-averaged gradients even in the presence of strong shock waves.

Under this new framework for constructing compact schemes, a series of high-order compact GKS are constructed on both structured and unstructured meshes through the design of high-order compact spatial reconstructions. In each cell, the cell-averaged flow variables and their gradients are provided to assist the compact reconstruction. The stencil of the compact spatial reconstruction only involves the nearest neighboring cells of the reconstruction cell, maintaining the consistency between the numerical and physical domains of dependence. To enhance the linear stability of the scheme, a least-squares method is generally employed for reconstruction, where the reconstructed polynomial is constrained by the cell-averaged gradients in a least-squares sense [9]. To handle discontinuities, adaptive nonlinear reconstruction, such as weighted essentially non-oscillatory (WENO) reconstruction [10, 11, 12, 9], is necessary. The nonlinear reconstruction employed in the present compact scheme is a newly proposed hybrid essentially non-oscillatory reconstruction method. However, as this is not the primary focus of this study, it will not be elaborated here.

The paper is structured as follows: Section 2 presents the framework of high-order compact GKS. Section 3 showcases the performance of the proposed compact scheme through a series of challenging numerical test cases. Finally, Section 4 concludes the paper.

2 High-Order Compact Gas-Kinetic Scheme

2.1 Solutions Update

The key to compact schemes lies in updating additional variables inside each mesh cell beyond just the cell averages of conservative variables, such as the derivatives or their equivalents. Unlike traditional methods that only compute fluxes of flow variables at cell interfaces, the proposed compact scheme directly evolves the flow variables at the interface, which is used to update the cell-averaged gradients, establishing a unique feature for the current high-order compact methods.

The update for cell averages is given by

$$\mathbf{W}_j^{n+1} = \mathbf{W}_j^n + \int_{t^n}^{t^{n+1}} \mathcal{L}_j(t)\mathrm{d}t, \tag{1}$$

where $\mathbf{W}_j$ is the cell-averaged flow variable defined as

$$\mathbf{W}_j \equiv \frac{1}{|\Omega_j|} \int_{\Omega_j} \mathbf{W}(\mathbf{x})\mathrm{d}V.$$

$\mathcal{L}_j(t)$ represents the net flux for cell j, whose definition and numerical discretization (Gaussian quadrature) are provided.

$$\mathcal{L}_j(t) = -\frac{1}{|\Omega_j|} \int_{\partial\Omega_j} \mathbf{F} \cdot \mathbf{n}\mathrm{d}S = -\frac{1}{|\Omega_j|} \sum_{l=1}^{l_0} \left(\sum_{k=1}^{q} \omega_k \mathbf{F}(\mathbf{x}_k) \cdot \mathbf{n}_l \right) |\Gamma_l|,$$

where $|\Gamma_l|$ is the face area of the cell, l_0 is the number of cell faces, $\mathbf{n}_l$ is the unit outer normal vector, and q and ω_k are the number of quadrature points and weight of the Gaussian quadrature rule.

Leveraging the modeled flow variables at cell interfaces, the update for cell-averaged gradients, determined via Gauss's theorem, is given by

$$\nabla\mathbf{W}_j^{n+1} \equiv \frac{1}{|\Omega_j|} \int_{\Omega_j} \nabla\mathbf{W}(\mathbf{x}, t^{n+1})\mathrm{d}V = \frac{1}{|\Omega_j|} \int_{\partial\Omega_j} \mathbf{W}(\mathbf{x}, t^{n+1})\mathbf{n}\mathrm{d}S. \tag{2}$$

Denoting the rightmost term in Eq.(2) as $\mathcal{M}$, its spatial discretization via numerical integration is given

as

$$\mathcal{M}_j^{n+1} = \frac{1}{|\Omega_j|} \sum_{l=1}^{l_0} \big(|\Gamma_l| \mathbf{n}_l \sum_{k=1}^{q} \omega_k \mathbf{W}^{n+1}(\mathbf{x}_k) \big),$$

where $\mathbf{W}^{n+1}(\mathbf{x}_k)$ is the value at the inner surface of Ω_j, which may be different from the value at the other side of the surface.

This study focuses on the construction of compact scheme with the numerical modeling of flow variables and fluxes. Details regarding linear spatial reconstruction can be found in the previous work [12, 9] and are omitted here for brevity.

2.2 Modeling the Flow Variables at Cell Interfaces

The distinct feature of the current compact method is the direct modeling of the flow variables at the cell interface. The evolution model for $\mathbf{W}(\mathbf{x}, t)$ at the cell interface is given by

$$\begin{aligned}
\mathbf{W}^l(\mathbf{x}, t) &= (1 - e^{-\Delta t/\tau_0})\mathbf{W}^e(\mathbf{x}, t) + e^{-\Delta t/\tau_0}\mathbf{W}_0^l(\mathbf{x}, t), \\
\mathbf{W}^r(\mathbf{x}, t) &= (1 - e^{-\Delta t/\tau_0})\mathbf{W}^e(\mathbf{x}, t) + e^{-\Delta t/\tau_0}\mathbf{W}_0^r(\mathbf{x}, t).
\end{aligned} \tag{3}$$

$\mathbf{W}^e$ is obtained by taking moments of the gas distribution function of GKS at the cell interface. Similarly, $\mathbf{W}_0^l$ and $\mathbf{W}_0^r$ are obtained by taking moments of the gas distribution functions, which depend solely on the initial reconstructions on the left and right sides, respectively. Details regarding the gas distribution function of the GKS, as well as the determination of flow variable and its time derivative from the gas distribution function can be found in [9, 13].
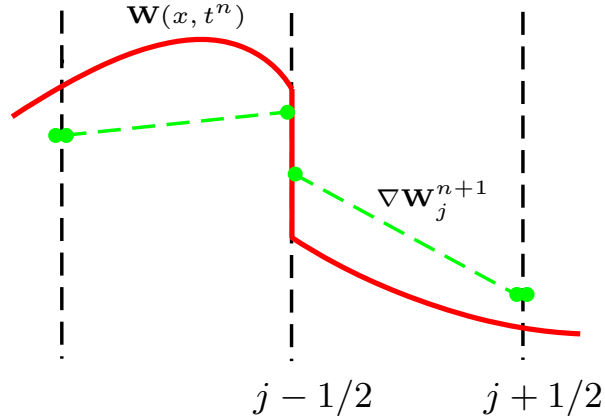

Figure 1: Schematic of flow variable evolution at the interface.

Fig.1 presents a schematic illustration of the direct numerical modeling for the flow variables at the cell interface, showcasing how the modeled interface values determine the cell-averaged gradients. The discontinuous nature of the evolution solution at the interface inherently captures the potential presence and propagation of a shock discontinuity across the interface within a single time step. The solutions of flow variables on both sides of the interface may become discontinuous in the general case. The weighting function $e^{-\Delta t/\tau_0}$ is constructed from a physical relaxation model, while in the smooth flow region under $\Delta t \gg \tau_0$, a continuous flow variable at the cell interface is recovered. The relaxation time τ_0 is defined as

$$\tau_0 = C \big| \frac{p_l - p_r}{p_l + p_r} \big| \Delta t,$$

where p_l and p_r are the pressures at both sides of the cell interface, and C is a constant coefficient with a value $C = 5$ in all test cases in this study. The same modeling of relaxation time in case of numerical shock wave is firstly proposed in GKS [13].

2.3 Time Discretization and Nonlinear Limiting in Time

This section presents the explicit time-marching method. By applying nonlinear limiting to the high-order terms of the numerical flux, a nonlinear 2-stage 4th-order (S2O4) method is constructed.

$$
\begin{aligned}
\mathbf{W}_j^{n+1/2} =& \mathbf{W}_j^n + \frac{\Delta t}{2}\mathcal{L}_j(\mathbf{W}^n) + \frac{\Delta t^2}{8}\mathcal{L}_{j,t}(\mathbf{W}^n), \\
\mathbf{W}_j^{n+1} =& \mathbf{W}^n + \Delta t\mathcal{L}_j(\mathbf{W}^n) + \frac{\Delta t^2}{2}\mathcal{L}_{j,t}(\mathbf{W}^n) \\
& - \frac{\Delta t^2}{3}\widetilde{\mathcal{L}}_{j,t}(\mathbf{W}^n) + \frac{\Delta t^2}{3}\widetilde{\mathcal{L}}_{j,t}(\mathbf{W}^{n+1/2}),
\end{aligned}
\tag{4}
$$

where in the second stage from t^n to t^{n+1} a nonlinear limiter for the higher-order time derivatives of the flux function is introduced [14]. The nonlinearly limited operator $\widetilde{\mathcal{L}}_j$ is defined as

$$
\widetilde{\mathcal{L}}_j(\mathbf{W}) = -\frac{1}{|\Omega_j|}\sum_{l=1}^{l_0}\omega_l^t\big(\sum_{k=1}^q\omega_k\mathbf{F}(\mathbf{x}_k)\cdot\mathbf{n}_l\big)\big|\Gamma_l\big|,
$$

where ω_l^t is a nonlinear weight for the lth interface of the cell and $\omega_l^t \in [0,1]$. The specific definition of ω_l^t can be found in [14]. The numerical flux and its time derivative in $\mathcal{L}_j$ and $\mathcal{L}_{j,t}$ are determined from the gas distribution function of GKS. A comprehensive presentation can be found in the previous work [9, 13].

Corresponding to the two-stage update in Eq.(4), the cell-averaged gradients are also updated in two stages.

$$
\begin{aligned}
\nabla\mathbf{W}_j^{n+1/2} &= \mathcal{M}_j^n + \frac{1}{2}\Delta t\mathcal{M}_{j,t}^n, \\
\nabla\mathbf{W}_j^{n+1} &= \mathcal{M}_j^n + \Delta t\mathcal{M}_{j,t}^{n+1/2}.
\end{aligned}
\tag{5}
$$

3 Numerical Examples

3.1 Advection of Entropy Wave in One Dimension

The test case involves the advection of a 1-D entropy wave in a stationary mean flow. The computational domain takes [-800, 1000] with free flow boundary conditions applied. The initial condition is

$$
(\rho, U, p) = (1 + 0.5e^{-\ln 2x^2/1.5^2}, 1, 1).
$$

This test is similar to the one presented in [15], where the linear advection equation is solved directly using high-order finite difference and DG schemes with a very small CFL number (CFL< 0.05). The computational time is $t = 400$.

For comparison, the result from a 6th-order DG-p5 scheme [15] using a cell size of 5, ensuring comparable degrees of freedom with the finite volume method, are presented in Fig. 2. This DG-p5 scheme requires updating six independent evolution equations in each cell and employs a CFL number of 1/30, achieving 4th-order accuracy through a 4-stage time marching method. In contrast, the compact GKS updates only one gas distribution function evolution equation at the cell interface to update both cell-averaged values and slopes, achieving 4th-order accuracy with a CFL number of 0.5 using a 2-stage time marching method. This difference highlights the efficiency of the compact GKS, even for smooth flows. Furthermore, the use of a coarse mesh to resolve the high-wavenumber entropy waves leads to noticeable numerical oscillations in the DG-p5 result, while the 6th-order compact GKS result remains oscillation-free.

3.2 Viscous Shock Tube Flow

The viscous shock tube problem, characterized by complex shock wave and boundary layer interaction, demands numerical methods with both robustness and accuracy. This study investigates this phenomenon within a unit square cavity, employing a symmetrical boundary condition at the top and
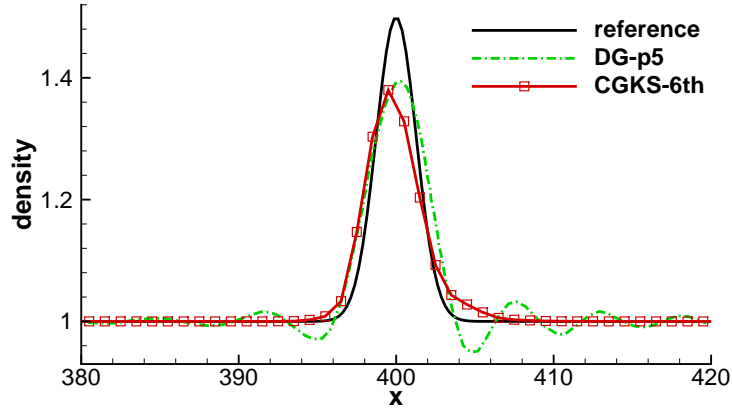
Figure 2: Advection of a 1-D entropy wave: the results are obtained at $t = 400$ by the 6th-order compact GKS and DG-p5 schemes after a long period of wave propagation.

non-slip adiabatic conditions on the remaining walls. The initial condition is

$$(\rho, U, V, p) = \begin{cases} (120, 0, 0, 120/\gamma), 0 \leq x < 0.5, \\ (1.2, 0, 0, 1.2/\gamma), 0.5 \leq x \leq 1. \end{cases}$$

The fluid viscosity is set at $\mu = 0.005$, resulting in a Reynolds number of $Re = 200$. The Prandtl number in the current computation is set to be $Pr = 1$. The specific heat ratio γ is 1.4. Initially, a shock wave, followed by a contact discontinuity, propagates towards the right wall, forming a thin boundary layer along the lower wall. This interaction ultimately leads to a lambda-shaped shock pattern after reflection from the right wall. The computational time is $t = 1$.

The left figure of Fig. 3 presents a local view of the triangular mesh with a cell size of 1/400, and the right figure of Fig. 3 shows the density contours at the final time, $t = 1$. The 4th-order compact GKS is adopted and it successfully captures both the vortex structures and the lambda shock with no discernible numerical oscillations near the shock front. The left figure of Fig. 4 illustrates the mesh convergence of the 4th-order compact GKS. As the mesh is refined, the density distribution along the lower wall obtained with the compact GKS approaches the reference solution, which is obtained using a non-compact high-order GKS on a very fine mesh [16]. The right figure of Fig. 4 compares the solution of the 4th-order compact GKS with the results obtained by the 3rd-order CPR method [17], both utilizing the gas distribution function of GKS for flux calculations. Notably, the 4th-order compact GKS achieves superior accuracy even on a coarser mesh compared to the 3rd-order CPR method. Moreover, the 4th-order compact GKS does not require any troubled-cell detection or non-linear limiting procedures.
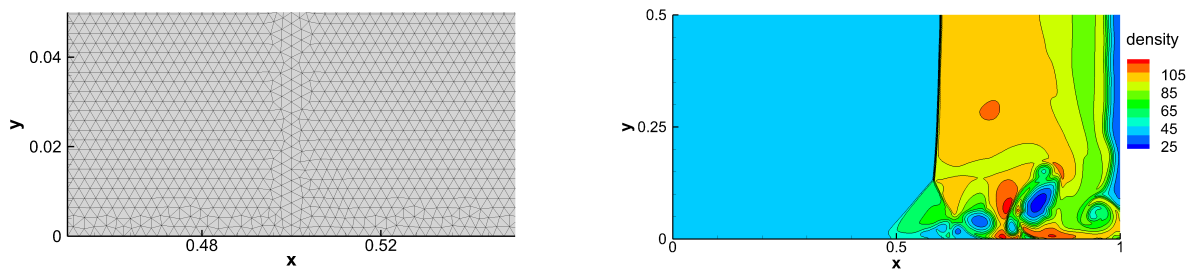

Figure 3: Viscous shock tube flow. Local computational mesh with cell size $h = 1/400$ and the density contours.
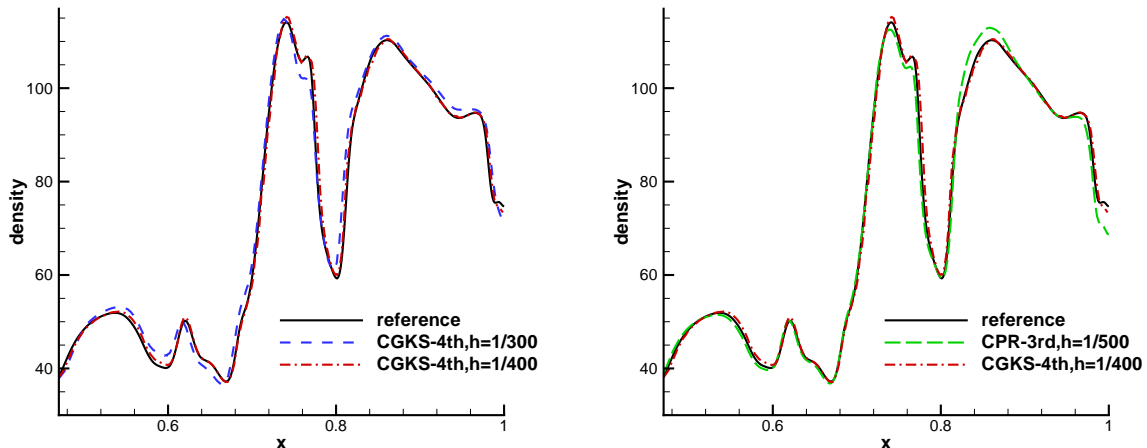
Figure 4: Viscous shock tube flow. The density distribution along the lower wall. The left figure shows results obtained using the 4th-order compact GKS on meshes with varying cell sizes. The right figure compares the 4th-order compact GKS and the 3rd-order CPR scheme, both utilizing the gas distribution function of GKS for flux calculations.

3.3 3-D Implosion Problem

The 3-D Noh problem [18], an implosion test modeling gas compression with a constant radial velocity towards a spherical center, is simulated on a computational domain of $[0, 0.3]^3$. The initial density and pressure are $\rho = 1$ and $p = 1 \times 10^{-4}$, and the velocity is $(U, V, W) = (-x, -y, -z)/\sqrt{x^2 + y^2 + z^2}$. The specific heat ratio is $\gamma = 5/3$. Inviscid wall boundary conditions are applied at $x = 0$, $y = 0$, and $z = 0$, while supersonic inflow boundary conditions, using the initial pressure, velocity, and analytical density solution, are imposed on the remaining boundaries. The analytical solution of density is given as

$$\rho = \begin{cases} 64, & r < t/3, \\ (1 + t/r)^2, & r > t/3. \end{cases}$$

The final computational output time is $t = 0.6$. The mesh consists of tetrahedral cells with an average side length of $h = 0.01$.

Fig. 5 displays the computational mesh and 3-D density contours. Fig. 6 presents density profiles along lines connecting the origin to $(0.3, 0.15, 0.15)$, $(0.15, 0.3, 0.15)$, $(0.15, 0.15, 0.3)$, and $(0.3, 0.3, 0.3)$ at a final time of $t = 0.6$. A large CFL number of CFL= 0.5 is used in the current computation without any additional limiting. The compact GKS accurately captures the strong shock wave, achieving a post-shock density profile comparable to that of a hybrid 5th- and 6th-order WENO scheme on a structured mesh with a five-times smaller mesh cell size [18]. Furthermore, simulations of this test case using other compact methods are scarcely reported in the literature.

4 Conclusion

This study presents a novel framework for constructing high-order compact schemes. Within the current framework, based on the time-accurate gas distribution function of the GKS, both the numerical fluxes and the flow variables at the cell interface are numerically modeled. These time-dependent solutions are employed to update the cell-averaged flow variables and their gradients. Two key ingredients are introduced to ensure both the robustness and high-order accuracy of the updating solutions. The evolution model accounts for the possibility of a shock discontinuity is located on or passes through a cell interface within a single time step. This is achieved by evaluating flow variables on both sides of the interface, enabling reliable updates of cell-averaged gradients when a shock wave appears and propagates at the cell interface. A nonlinear limiting procedure, analogous to spatial WENO schemes, is applied to the high-order time derivative of the flux function within the multi-stage multi-derivative time-stepping method. This mitigates the possible spurious oscillations as a shock traverses a cell interface during a
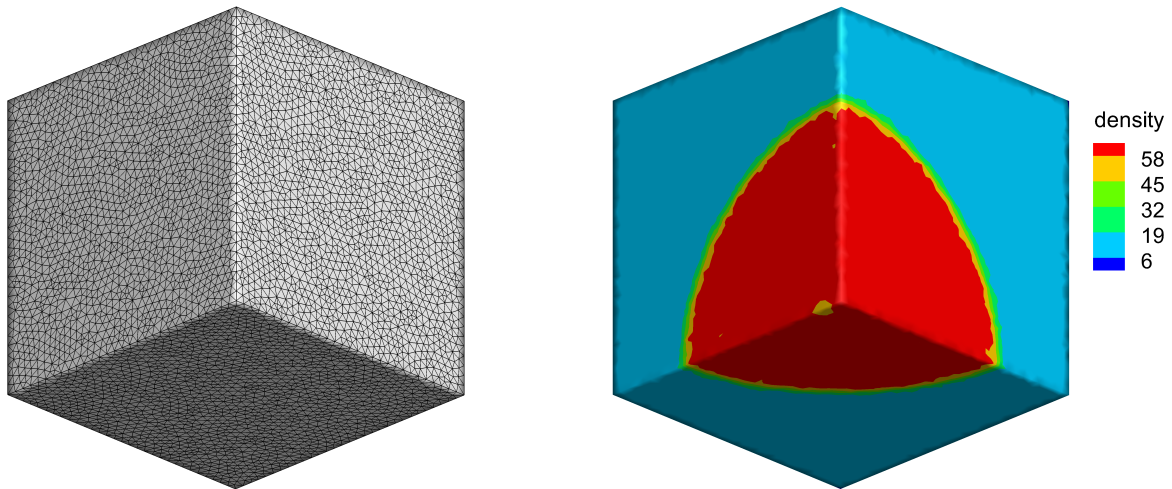
Figure 5: 3-D Implosion Problem: the tetrahedral mesh (left) and density contours (right) by 4th-order compact GKS of Noh problem at $t = 0.6$. The average side length of cells of the tetrahedral mesh is $h = 0.01$.
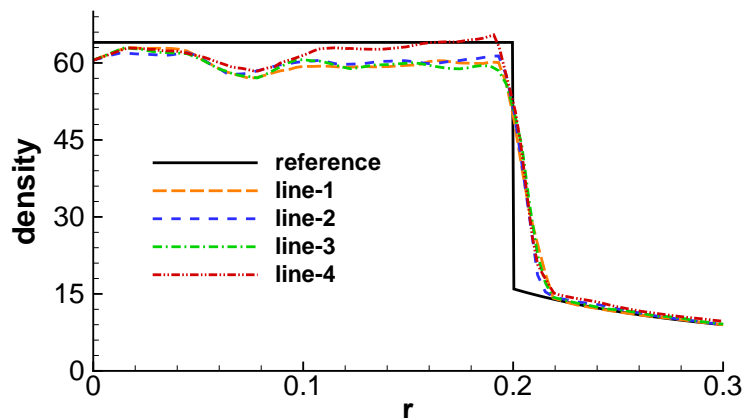

Figure 6: 3-D Implosion Problem: the density distribution along lines by 4th-order compact GKS of Noh problem at $t = 0.6$. The average side length of cells of the tetrahedral mesh is $h = 0.01$.

time step. A series of high-order compact GKS schemes have been constructed on both structured and unstructured meshes through high-order compact spatial reconstructions. The superior robustness and accuracy of these compact schemes are demonstrated through a series of challenging numerical test cases.

References

[1] William H Reed and Thomas R Hill. Triangular mesh methods for the neutron transport equation. Technical report, Los Alamos Scientific Lab., N. Mex.(USA), 1973.

[2] Bernardo Cockburn and Chi-Wang Shu. Tvb runge-kutta local projection discontinuous galerkin finite element method for conservation laws. ii. general framework. *Mathematics of computation*, 52(186):411–435, 1989.

[3] Chi-Wang Shu. High order weno and dg methods for time-dependent convection-dominated pdes: A brief survey of several recent developments. *Journal of Computational Physics*, 316:598–613, 2016.

[4] Hung T Huynh. A flux reconstruction approach to high-order schemes including discontinuous galerkin methods. In *18th AIAA computational fluid dynamics conference*, page 4079, 2007.

[5] Zhi Jian Wang and Haiyang Gao. A unifying lifting collocation penalty formulation including the

discontinuous galerkin, spectral volume/difference methods for conservation laws on mixed grids. *Journal of Computational Physics*, 228(21):8161–8186, 2009.

[6] Sanjiva K Lele. Compact finite difference schemes with spectral-like resolution. *J. Comput. Phys.*, 103:15, 1991.

[7] Xiaogang Deng and Hanxin Zhang. Developing high-order weighted compact nonlinear schemes. *Journal of Computational Physics*, 165(1):22–44, 2000.

[8] Qian Wang, Yu-Xin Ren, Jianhua Pan, and Wanai Li. Compact high order finite volume method on unstructured grids iii: Variational reconstruction. *Journal of Computational physics*, 337:1–26, 2017.

[9] Fengxiang Zhao, Xing Ji, Wei Shyy, and Kun Xu. A compact high-order gas-kinetic scheme on unstructured mesh for acoustic and shock wave computations. *Journal of Computational Physics*, 449:110812, 2022.

[10] Xu-Dong Liu, Stanley Osher, and Tony Chan. Weighted essentially non-oscillatory schemes. *Journal of computational physics*, 115(1):200–212, 1994.

[11] Guang-Shan Jiang and Chi-Wang Shu. Efficient implementation of weighted eno schemes. *Journal of computational physics*, 126(1):202–228, 1996.

[12] Fengxiang Zhao, Xing Ji, Wei Shyy, and Kun Xu. Compact higher-order gas-kinetic schemes with spectral-like resolution for compressible flow simulations. *Advances in Aerodynamics*, 1(1):13, 2019.

[13] Kun Xu. A gas-kinetic bgk scheme for the navier–stokes equations and its connection with artificial dissipation and godunov method. *Journal of Computational Physics*, 171(1):289–335, 2001.

[14] Fengxiang Zhao, Xing Ji, Wei Shyy, and Kun Xu. Direct modeling for computational fluid dynamics and the construction of high-order compact scheme for compressible flow simulations. *Journal of Computational Physics*, 477:111921, 2023.

[15] Ziqiang Cheng, Jinwei Fang, Chi-Wang Shu, and Mengping Zhang. Assessment of aeroacoustic resolution properties of dg schemes and comparison with drp schemes. *Journal of Computational Physics*, 399:108960, 2019.

[16] Qibing Li, Kun Xu, and Song Fu. A high-order gas-kinetic navier–stokes flow solver. *Journal of Computational Physics*, 229(19):6715–6731, 2010.

[17] Chao Zhang, Qibing Li, Song Fu, and Zhi Jian Wang. A third-order gas-kinetic cpr method for the euler and navier–stokes equations on triangular meshes. *Journal of Computational Physics*, 363:329–353, 2018.

[18] Eric Johnsen, Johan Larsson, Ankit V Bhagatwala, William H Cabot, Parviz Moin, Britton J Olson, Pradeep S Rawat, Santhosh K Shankar, Björn Sjögreen, Helen C Yee, et al. Assessment of high-resolution methods for numerical simulations of compressible turbulence with shock waves. *Journal of Computational Physics*, 229(4):1213–1237, 2010.